Skeletal muscle mitoribosomal defects are linked to low bone mass caused by bone marrow inflammation in male mice

JINGWEN TIAN[1,3,#], Hyo Kyun Chung[2,#], Ji Sun Moon[2,3], Ha Thi Nga[1,3], Ho Yeop Lee[1,3], Jung Tae Kim[1,2], Joon Young Chang[1,2], Seul Gi Kang[1,2], Dongryeol Ryu[4,5], Xiangguo Che[6,7], Je-Yong Choi[6], Masayuki Tsukasaki[8], Takayoshi Sasako[9], Sang-Hee Lee[10], Minho Shong[1,2], and Hyon-Seung Yi[1,2,3 *],

*Corresponding author: Hyon-Seung Yi, Research Center for Endocrine and Metabolic Diseases, Chungnam National University School of Medicine, Daejeon 35015, Korea. **Phone**: +82-42-280-6994; **Fax**: +82-42-280-6990; **E-mail**: jmpbooks@cnu.ac.kr

Supplementary methods

Human subjects

Patients with hip fracture were recruited from the Chungnam National University Hospital between October 2019 and February 2020. The participants were divided into two age- and gender-matched groups as follows: body mass index (BMI) 22–25 (n = 7) and BMI <18 (n = 7). Patients with any of the following conditions were excluded from the study: rheumatoid arthritis, neuromuscular disorders, chronic kidney disease, and mineral and bone disorders. Patients with diseases that affect bone metabolism (or those taking drugs that affect bone metabolism), with a history of any malignant or inflammatory disease, and past hormone replacement therapy were also excluded. Hand grip strength was measured using an electronic hand dynamometer (Lavisen, Namyangju, South Korea). Grip strength of the dominant hand was measured only once, in a sitting posture with 0° shoulder angle, 90° elbow angle, and a neutral wrist angle. Lymphocytes were isolated from the bone marrow (BM) cells of the enrolled patients and stored at -180°C in liquid nitrogen prior to flow cytometry analysis. Muscle tissues from the *vastus lateralis* were used for immunoblots. Whole BM cells were used for real-time PCR analysis. This human study was reviewed and approved by the Institutional Review Board of Chungnam National University Hospital (CNUH 2019-10-065), according to the standards of the Declaration of Helsinki. Written and oral informed consent, documented by the Department of Internal Medicine of Chungnam National University Hospital in South Korea, was obtained from all of the participants prior to their inclusion in the study.

Immunoblot analysis

Tissues and cells were lysed in 2% sodium dodecyl sulfate (SDS) with 2 M urea, 10% glycerol, 10 mM Tris-HCl (pH 6.8), 10 mM dithiothreitol, and 1 mM phenylmethylsulfonyl fluoride. The lysates were centrifuged and the supernatants were separated by SDS-polyacrylamide gel electrophoresis (PAGE). Proteins were transferred to a nitrocellulose (NC) membrane. After blocking with 5% skimmed milk, the membrane was probed using specific antibodies (see Table S2) A horseradish peroxidase-conjugated goat anti-rabbit IgG (Enzo Life Sciences, Farmingdale, NY, USA)

secondary antibody was used for visualization and visualized by enhanced chemiluminescence using WesternBright ECL Spray (Advansta, Menlo Park, CA, USA). . Signals were scanned using an Odyssey imager and Image Studio Software (LI-COR Biosciences, Lincoln, NE, USA). Target protein levels were normalized to those of glyceraldehyde 3-phosphate.

BN-PAGE

To isolate mitochondria from the EDL and gastrocnemius muscle of 14-week-old control and MKO mice, samples were homogenized in isolation buffer (210 mM mannitol, 70 mM sucrose, 1 mM EGTA, and 5 mM HEPES, pH 7.2) using a Teflon-glass homogenizer. The homogenized tissues were centrifuged at 600 × g for 5 min at 4°C, and the supernatant was re-centrifuged at 17,000 × g for 10 min at 4°C. The isolated mitochondrial fraction was supplemented with 0.5% (w/v) n-dodecyl-β-D-maltoside and assessed for OxPhos complex content using a Native PAGE Novex Bis-Tris Gel system (Invitrogen, Carlsbad, CA, USA). The separated proteins were transferred to polyvinylidene fluoride membranes, which were incubated overnight at 4°C with an anti-OxPhos antibody cocktail (Invitrogen, #45-8099, #45-7999), followed by analysis using the Western Breeze Chromogenic Western Blot Immunodetection Kit (Invitrogen).

Immunohistochemistry

Transverse 12 μm muscle sections were mounted on Super Frost microscope slides (Thermo Fisher Scientific, Waltham, MA, USA). Muscle fiber type-specific diameter measurements were obtained at 14 weeks-of-age using 12 μm-thick SDH-stained cross-sections. Sections were outlined with a PAP pen (Research Products International) and incubated for 45 min at room temperature in buffer solution (20 mM phosphate buffer, 7.5% sucrose, 0.027% sodium succinate, and 10 mg nitrobluetetrazoleum). The sections were dehydrated and then rinsed briefly in 30%, 60%, and 90% acetone/distilled water in ascending and then descending order. Finally, they were rinsed in distilled water, air-dried, and cover-slipped using VectaMount (Vector Labs).

For laminin and Myosin heavy chain Type IIB (MyHC2b) staining, muscle tissue was embedded in FSC 22 Frozen Media (Leica Biosystems, IL, USA). Transverse (7 μm) muscle sections were incubated overnight at 4ºC with rabbit anti-laminin (Abcam, ab11575 1:500 dilution) and mouse anti-MyHC type 2b (DSHB, BF-F3, 1:500 Dilution) antibodies in 5% goat serum blocking solution, and then washed three times with 1X PBS. Finally, sections were incubated for 45 minutes with Alexa Fluor 488 goat anti-rabbit IgG (Invitrogen, 1:1000 Dilution) and Alexa Fluor 555 goat anti-mouse IgG (Invitrogen, 1:1000 Dilution).

Micro-CT analysis

Micro-CT was performed on vertebrae and long bones using an eXplore Locus SP scanner (GE Healthcare, London, Canada) with 8 μm resolution. All bone morphometric parameters were calculated three-dimensionally by eXplore MicroView version 2.2 (GE Healthcare), which was used for measuring number of trabecular (Tb.N) , bone volume/total volume (BV/TV), trabecular thickness (Tb.Th), and trabecular separation (Tb.Sp), cortical volume (Ct.V), cortical thickness (Ct.Th). Bone parameters and density were analyzed at the region between 0.7 and 2.3 mm below the growth plate of the distal femur. Cancellous bone was analyzed in the distal area extending proximally 1.75 mm from the end of the primary spongiosa. All bone micro-CT nomenclature follows the guidelines of the American Society for Bone and Mineral Research (ASBMR).

Mouse grip strength and wire hanging test

Experiments were performed using a digital force-gauging apparatus (GS 5000; Borj Sanat, Iran). Mice were allowed to grasp the pull bar with the forelimbs. Then, they were pulled gently away from the bar by the tail until they released the bar. Mice were not trained before testing. The maximum force prior to release of the mouse's paw from the bar was recorded. The test was repeated five times, and the average value of five consecutive measurements was reported as the mouse's "grip strength". The wire hanging test was conducted to assess motor function and neuromuscular grip strength. The mouse was placed on a cross-grip wire rack, which was then turned upside down 20 cm above a cage

filled with soft bedding, after which hanging time was recorded. The average latency to fall of four trials was calculated for each animal. The maximum hanging time was used in the analyses.

RNA sequencing

Total RNA was prepared from EDL and BM cells obtained from 10-week-old control and MKO mice (n = 2 for each) using TRIzol reagent. The integrity of the total RNA was assessed using an Agilent 2100 Bioanalyzer System (Agilent Technologies, Loveland, CO, USA) and an Agilent RNA 6000 Nano Kit (Agilent Technologies, Loveland, CO, USA). The library was prepared using a TruSeq 3000/4000 SBS Kit, v3. Pre-processed the raw reads from the sequencer to remove results from low-quality RNA or artifacts such as adaptor sequences, contaminant DNA, and PCR duplicates. The quality of the data produced is determined by the phred quality score for each base. The FastQC quality control tool gives a box plot of average base quality per cycle; a phred quality score of 20 means that the assignment to that base is 99% accurate. Generally a phred score ≥20 denotes good quality: 97.19% of those in the present study were ≥30. The obtained reads were mapped to a reference Mus musculus (mm10) genome using HISAT2 v2.0.5. HISAT uses two types of index for alignment (a global, whole-genome index and tens of thousands of small local indices). These aligned reads were then assembled from known genes/transcripts using a reference gene model in StringTie v.1.3.3b. Transcript frequencies were quantified as normalized values, taking into account transcript length and depth of coverage. Relative transcript abundance was expressed as fragments per kilobase of transcript per million fragments mapped (FPKM), and FPKM values ≤0 were excluded. One was added to each FPKM value for filtered genes, the filtered data were log2-transformed, and quantile normalization was applied. Differentially expressed gene (DEG) analysis was performed using FPKM values. Genes with a fold change >2 and an independent t-test P-value <0.05 were extracted from the results of DEG analysis. A heatmap was produced by color-coding standardized log gene expression levels (mean, zero; standard deviation, one) using R 3.5.1 available at http://www.r-project.org. Probe sets are shown as hierarchically clustered by similarity, based on Euclidean distance and the Ward aggregation algorithm.

RNA sequencing analysis using bioinformatics tools

DEGs were then subjected to hierarchical clustering and phenotype ontology using Network2Canvas (http://maayanlab.net/N2C/). Phenotype categories were visualized on the grid according to gene-list similarity, with enriched categories being indicated by circles. Gene Set Enrichiment Analysis (GSEA) (http://www.broadinstitute.org/gsea) was performed using transcriptome data from the BM cells from control and MKO mice. Bioinformatic analysis was carried out with R package v3.2.5, available at http://www.r-project.org. A heatmap was produced by color-coding standardized log gene expression levels (mean, zero; standard deviation, one). Probe sets are shown as hierarchically clustered by similarity, based on Euclidean distance and the Ward aggregation algorithm. We also used G-MAD in GeneBridge tools (available at http://systems-genetics.org, an open resource), which uses expression data from large-scale cohorts to propose potential functions of genes and allows the annotation of gene function.

Treatment with AMD3100 *in vivo*

Control and MKO mice (9 weeks-of-age) were injected intraperitoneally with 5 mg/kg PBS or AMD3100 (Sigma-Aldrich #A5602; St. Louis, MO, USA; Sigma-Aldrich.com), three times per week for 3 weeks. At the end of treatment, the mice were sacrificed and blood samples were collected for measurement of proinflammatory cytokines and markers of bone turnover. Femurs and tibiae were removed, fixed with 4% paraformaldehyde in PBS solution (pH 7.4) for 16 h, and then stored at 4°C in 80% ethanol prior to measurement of bone mineral density (BMD) using micro-CT.

Serum measurements.

Blood samples were collected by cardiac puncture of mice under general anesthesia. Samples were centrifuged at 10,000 rpm for 5 min, and the supernatant was used for assaying triglycerides, total cholesterol, alanine aminotransferase, and aspartate transaminase using a DRI-CHEM 4000i automated system (Fujifilm, Tokyo, Japan). Serum levels of TNF-α and IL-17A were determined using a specific enzyme-linked immunosorbent assay (ELISA; TNF-α, BD Bioscience, NJ, USA; IL-17A, Sigma-

Aldrich, St. Louis, MO, USA) following the manufacturer's protocol. C-telopeptide (CTX), procollagen type 1 N propeptide (P1NP), testosterone, T3, and T4 were measured by ELISAs. Serum levels of T3, T4, and testosterone were measured using an ELISA kit (T3 and T4, Merck-Millipore, Darmstadt, Germany; testosterone, ALPCO, Salem, NH, USA). Serum parathyroid hormone (PTH) levels were measured using the mouse intact PTH ELISA kit (Immutopics International, San Clemente, CA, USA). Serum FGF21 and GDF15 levels were assayed with a commercial ELISA kit (R&D Systems, Minneapolis, MN, USA).

Preparation of BM cells from mice and humans

Control and MKO mice (14 weeks-of-age) were anesthetized by intraperitoneal injection of sterile avertin (tribromoethanol: 200 mg/10 ml/kg), and then tibias and fibulas were removed. The BM cells were flushed from the medullary cavities of the excised bones and suspended in RPMI-1640 medium containing 10% fetal bovine serum (FBS). Human BM cells were isolated from patients who underwent hip arthroplasty at the Chungnam National University Hospital between October 2019 and February 2020. The BM cells were extracted from the femoral neck cutting area without bacterial contamination, and were subjected to flow cytometry and real-time PCR analysis. The demographic and clinical characteristics of the patients with a BMI of <18 kg/m^2 and 22–25 kg/m^2 that were included in this study are shown in Table S1.

RNA extraction and real-time PCR analysis.

Total RNA was extracted from the BM cells using TRIzol reagent (Life Technologies, Eugene, OR, USA). Complementary DNA (cDNA) was synthesized from total RNA using M-MLV reverse transcriptase and oligo-dT primers (Invitrogen, Carlsbad, CA, USA). Specific sequences were amplified from each cDNA sample using SYBR Green PCR Master Mix (Applied Biosystems, Foster City, CA, USA) and specific primers (Tables S3, 4) using a 7500 Real-Time PCR System and Software, v2.0.6 (Applied Biosystems). The comparative Ct method was used to determine relative expression, with 18s ribosomal RNA as the reference gene.

Measurement of BMD in human subjects.

BMD was measured in the lumbar spine (1st–4th lumbar vertebrae) and femoral neck of the participants with hip fracture using dual energy X-ray absorptiometry with a Discovery (Hologic Inc., Marlborough, MA, USA) scanner. All BMD scans were conducted by well-trained examiners using standardized procedures following the manufacturer's recommended protocols. The lumbar BMD of 30 patients was measured with two consecutive measurements per patient. Any scans comprising metal or other attenuating material in the region of interest, as well as any scans of poor quality were discarded. The precision error of the lumbar BMD measurement was 1.4%, which was lower than the minimum acceptable precision error of 1.9% for the lumbar spine.

Rotarod test of coordination.

Mice were trained at 10 rpm on an Economex rotarod fitted with a 3 cm-diameter rod (Columbus Instruments, Columbus, OH, USA), and the latency to fall (maximum 60 s) was measured to evaluate motor coordination and balance. Fixed speed rotarod assessment was performed at a constant speed of 10 rpm with a 300 s maximum time limit. After acclimation, all mice received training for 2 consecutive days. On the test day, the mice were tested in three consecutive trials of 1 min each, with 1 min rest between trials. The latency to fall during each of the three trials was averaged to give the overall time for each mouse.

Measurement of grip strength in human subjects.

Grip strength was measured using a digital handheld dynamometer in a sitting position with elbows unsupported forming an angle of 90° (Lavisen, Hanam, Korea). Participants were asked to apply the maximum grip strength three times in the dominant hand. Between each measurement, at least 30 s of rest was allowed. Grip strength was defined as the maximally measured grip strength of the dominant hand.

Transmission electron microscopy

Gastrocnemius muscle samples from mice were fixed in 1% (wt/vol) glutaraldehyde at 4°C and then washed with 0.1 M cacodylate buffer, pH 7.2, at 4°C. Washed muscle tissues were fixed for 1 h at 4°C with 1% (wt/vol) OsO4 in 0.1 M cacodylate buffer, pH 7.2, containing 0.1% (wt/vol) $CaCl_2$. Muscle samples were dehydrated by graded series of ethanol and propylene oxide treatment, and then embedded in Embed-812 (Electron Microscopy Sciences). The resin blocks were then polymerized at 60°C for 48 h. Tissues were sectioned with an EM UC6 ultramicrotome (Leica Microsystems, Vienna, Austria) and post-stained with 4% (wt/vol) uranyl acetate and citrate. Specimens were observed on a JEM ARM 1300S high-voltage electron microscope (JEOL, Japan).

In vitro osteoclastogenesis

Femurs were removed aseptically from 8–9-week-old C57BL/6J mice and BM cells were flushed out with a sterile 21-gauge syringe. The cells were cultured in alpha-MEM containing 10% FBS and 30 ng/mL M-CSF (R&D Systems, Minneapolis, MN, USA). After 2 days, adherent cells were used as bone marrow-derived monocyte/macrophages. To generate osteoclasts, these cells were further cultured in the presence of 30 ng/mL of RANKL and 10 ng/mL of M-CSF with or without recombinant CXCL12 (5 ng/mL). After 3 days, the cells were fixed and stained for tartrate-resistant acid phosphatase (TRAP) using the TRAP staining kit (Sigma-Aldrich, St. Louis, MO, USA), and the number of TRAP-positive multinucleated (> 3 nuclei) cells (MNCs) and TRAP-positive larger (> 100 μm) MNCs were counted.

Osteoblast experiment

Murine pre-osteoblastic MC3T3-E1 cells were purchased from the American Tissue Culture Collection. The cells were cultured in alpha-MEM containing 10% FBS, ascorbic acid (50 μg/mL), β-glycerophosphate (5 mM), and recombinant BMP2 (100 μg/mL) with or without recombinant CXCL12 (5 ng/mL) to induce osteoblast differentiation. After 5 days, the cells were fixed and stained with alkaline phosphatase to detect osteogenic differentiation.

T-cell activation

BM cells were isolated from femurs of 8–9 week-old C57BL/6J mice. The cells were seeded in 24-well plates and cultured in RPMI-1640 medium containing 10% FBS with or without recombinant CXCL12 (5 ng/mL). After 24 h, floating cells were collected, stimulated for 5 h with Cell Stimulation Cocktail (eBioscience, San Diego, CA, USA), and then harvested. The cells were fixed and permeabilized using Fixation/Permeabilization Buffer kit (eBioscience, San Diego, CA, USA), and then stained for intracellular cytokines with anti-TNF-α-APC and anti-IL-17A-PE antibodies. Multicolor flow cytometry was performed using a LSRFortessa flow cytometer (BD Biosciences, NJ, USA), and the data were analyzed using FlowJo software (Tree Star, Ashland, OR, USA). Results are expressed as cell frequency (%).

Supplementary figure legends

Fig. S1 Generation of the skeletal muscle-specific mitochondrial oxidative phosphorylation (OxPhos) dysfunction mouse model. (A) Strategy for generating MKO mice through disrupting *Crif1* in skeletal muscle using the MLC1f (myosin light chain 1f)-Cre mice through Cre-LoxP system. (B, C) Immunoblotting and band density measurement of OxPhos complex subunits in soleus muscle from 14-week-old control and MKO mice, $n = 3$. (D) Mitochondrial morphology of controls and MKO mice, visualized by electron microscopy; scale bars: 1 μm. (E, F) Immunoblotting and band density measurement of CRIF1 and OxPhos; complex subunits in BM and cortical bone of femur from 14-week-old control and MKO mice, n=3. (G) Body weight evolution of control and MKO mice fed a chow diet for 8 weeks, $n = 10$ per group. Data are expressed as the mean ± SEM. Statistical significance was analyzed by unpaired t-tests. **, $P < 0.01$ compared with the indicated group.

Fig. S2 Micro-CT analysis of vertebrae and femurs of control and MKO mice at 14 weeks-of-age. (A) The cortical area in femurs of control and MKO mice were measured by micro-CT. (B) Cortical bone area/total tissue area (Ct.Ar/Tt.Ar; %) was measured in femurs of control and MKO mice. (C, D) Measurement of bone volume (BV)/total volume (TV) using von Kossa staining of vertebrae and femurs from 14-week-old control and MKO mice, $n = 5$. (E, F) Quantitative analysis of eroded surface per bone surface (%) and osteoclast surface (%) of tibiae from 14-week-old control and MKO mice, $n = 4$. Data are expressed as the mean ± SEM. Statistical significance was analyzed by unpaired t-tests. *, $P < 0.05$ and **, $P < 0.01$ compared with the indicated group.

Fig. S3 Measurement of serum levels of hormones affecting bone metabolism in control and MKO mice. (A-D) Serum concentrations of intact parathyroid hormone (iPTH), testosterone, T4, and T3 in 14-week-old control and MKO mice, $n = 7$/group. Data are expressed as the mean ± SEM.

Fig. S4 FGF21 is highly induced by mitochondrial stress in skeletal muscle of MKO mice. (A) Scatterplots of RNA sequencing data, displaying transcript levels in EDL of control (x-axis) and MKO (y-axis) mice at 10 weeks-of-age. The text indicates that mitokines show much higher fold change in MKO mice. (B, C) Volcano plot and heat map showing upregulated genes in EDL from normal chow diet-fed control and MKO mice at 10 weeks-of-age. (D) Relative expression of mRNA encoding *Fgf21* in EDL from 14-week-old control and MKO mice, $n = 6$. (E) Serum levels of FGF21 in 14-week-old control and MKO mice, $n = 6$. (F) Strategy for generating FGF21/CRF1 double knockout mice (MFKO) and genotype analysis using real-time PCR. (G) *Crif1* and *Fgf21* expression in the extensor digitorum longus muscle of MKO and MFKO mice at 6 weeks-of-age. Data are expressed as the mean ± SEM. **, $P < 0.01$ compared with the corresponding controls.

Fig. S5 Lower bone mass in MKO mice is independent of FGF21 production caused by mitochondrial stress in skeletal muscle. (A) Micro-CT images of the trabecular bone (Tr.b) near the distal femoral metaphyseal region of control and MKO mice at 14 weeks-of-age. Scale bar for the front view and 3D image of the Tr.b = 1000 and 500 μm, respectively; n = 4. (B) Measurement of Tb.Th., Tb.N., BV/TV, BS/TV, BS/BV, Ct.V., Tb.Sp., and TBV using micro-CT analysis. Data are expressed as the mean ± SEM. Statistical significance was analyzed by unpaired t-tests.

Fig. S6 Measurement of serum levels of proinflammatory cytokines in 14-week-old control and MKO mice. (A) Serum TNF-α and IL-17A concentrations in control ($n = 7$) and MKO ($n = 7$) mice at 14 weeks-of-age. (B) A representative section of tibia from a 14-week-old control and MKO mouse stained with H&E. Adipocyte-rich BM (arrowhead) are visible in the MKO mice. Scale bars, 100 μm. Quantification of the number of adipocytes per bone marrow surface area (mm^2) in control ($n = 4$) and MKO ($n = 4$) mice at 14 weeks-of-age. Data are expressed as the mean ± SEM. **, $P < 0.01$ compared with the corresponding controls.

Fig. S7 Analysis of RNA sequencing data from BM cells of control and MKO mice. (A, B) The analysis was performed using Network2Canvas. Genes that were significantly upregulated in the BM cells of control and MKO mice were analyzed for gene-list enrichment, with gene set libraries created

from level 4 of the MGI mouse phenotype ontology using Network2Canvas. (C) *Cxcl12* mRNA expression by BM cells from control and MKO mice at 14 weeks-of-age. (D) In the G-MAD analysis, CXCL12 associates with T-cell proliferation and CXCR chemokine receptor binding modules in mice. The threshold of significant gene-module association is indicated by the red dashed line. Modules are organized by module similarities. Known modules connected to CXCL12 are highlighted in red. Data are expressed as mean ± SEM. *, $P < 0.05$ and **, $P < 0.01$ compared with the corresponding controls.

Fig. S8 Flow cytometry analysis of BM cells from 12-week-old control and MKO mice treated with or without AMD3100. (A) Populations of CD4+ and CD8+ T-cells from control and MKO mice treated with or without AMD3100 for 3 weeks. (B-E) IFN-γ- and TNF-α-producing CD4+ and CD8+ T-cells in the BM from control and MKO mice treated with or without AMD3100 for 3 weeks. (F) Statistical analysis of phenotypes defined by flow cytometry in the BM from control and MKO mice treated with or without AMD3100 for 3 weeks. Data are expressed as mean ± SEM. Statistical significance was analyzed by one-way ANOVA. *, $P < 0.05$ and **, $P < 0.01$ compared with the indicated group.

Fig. S9 Micro-CT analysis and measurement of serum markers of liver injury and lipid metabolism. (A,B) Cortical bone area/total tissue area (Ct.Ar/Tt.Ar; %) was measured in tibia and femurs of control and MKO mice treated with or without AMD3100. (C-F) Serum levels of aspartate transaminase (AST), alanine aminotransferase (ALT), total cholesterol (CHOL), and triglyceride (TG) from 12-week-old control and MKO mice treated with or without AMD3100. Data are expressed as mean ± SEM. Statistical significance was analyzed by one-way ANOVA. *, $P < 0.05$ and **, $P < 0.01$ compared with the indicated group.

Fig. S10 Grip strength and flow cytometry analysis of BM cells of patients with hip fracture. (A) Measurement of grip strength of the hip fracture patients using a handheld dynamometer. (B) Representative blots showing BN-PAGE of the assembled OxPhos complex in vastus lateralis muscle from patients with lower (<18 kg/m^2) or normal (22–25 kg/m^2) BMI. (C) Populations of CD4+ and CD8+ T-cells from the hip fracture patients with lower (<18 kg/m^2) or normal (22–25 kg/m^2) body mass index (BMI). (D, E) Naïve (CD45RA+CD45RO-) and memory (CD45RA-CD45RO+) CD4+ and CD8+ T-cells in the BM from the hip fracture patients with lower or normal BMI. (F) BM senescent (CD28-CD57+) CD4+ and CD8+ T-cells from hip fracture patients with lower (<18) or normal (22–25) BMI. (G-J) Transcript levels of *CXCL12*, *CD44*, *TNF*, and *IL17A* in the BM from hip fracture patients with lower (<18) or normal (22–25) BMI. Data are expressed as mean ± SEM. *, $P < 0.05$ and **, $P < 0.01$ compared with the corresponding controls.

Fig. S11 Serum levels of mitokines in patients with hip fracture. (A, B) Serum FGF21 and GDF15 levels were measured in hip fracture patients with lower (<18 kg/m^2) or normal (22–25 kg/m^2) BMI. Data are expressed as the mean ± SEM. *, $P < 0.05$ compared with the corresponding controls.

Supplementary tables

Table S1. Demographics and baseline characteristics of the human subjects

BMI (kg/m^2)	No.	Gender	Age (years)	BMI	Grip strength (Kg)	T score	Hip fracture site
22–25	1	M	75	22.73	31.6	-1.9	Lt. intertrochanter
	2	F	68	24.9	22.5	-2.4	Rt. neck
	3	M	69	23.1	28.9	-1.7	Rt. neck
	4	F	66	23.5	19.3	-2.9	Lt. intertrochanter
	5	M	61	24.6	30.5	-2.2	Rt. intertrochanter
	6	M	77	22.8	33.2	-1.8	Lt. neck
	7	M	72	24.2	27.3	-2.5	Lt. neck
<18	1	M	78	17.6	25.3	-2.2	Rt. neck
	2	M	61	17.1	23.6	-2.6	Rt. intertrochanter
	3	M	80	17.5	21.2	-2.9	Rt. intertrochanter
	4	M	66	16.8	26.9	-2.6	Lt. neck
	5	M	65	17.3	24.4	-2.8	Rt. neck
	6	F	72	17.6	15.2	-3.6	Lt. neck
	7	F	70	16.5	13.6	-3.8	Lt. intertrochanter

BMI, body mass index.
Lt, left.
Rt, right.

317 **Table S2. Antibodies used for flow cytometry analysis**

Antibody target/reagent	Fluorochrome	Clone	Supplier	Cat. No.
Fc block		2.4G2	BD Bioscience	553142
Fixable viability dye	APC-Cy7		eBioscience	65-0865
hCD4	Alexa Fluor 700	RPA-T4	eBioscience	56-0049
hCD8a	PE	RPA-T8	eBioscience	12-0088
hCD8a	APC	RPA-T8	eBioscience	17-0088
hCD3	PerCP-Cy5.5	SK7	eBioscience	46-0036
hCD3	PE-Cy7	UCHT1	eBioscience	25-0038
hCD57	FITC	TB01	eBioscience	11-0577
hCD28	APC	CD28.2	eBioscience	17-0289
hIFNG	PE-Cy7	4S.B3	eBioscience	25-7319
hTNFA	APC	MAb11	eBioscience	17-7349
hIL17A	APC	eBio64DEC17	eBioscience	17-7179
mIL17A	PE	eBio17B7	eBioscience	12-7177
mTNF-α	PerCP-eF710	MP6-XT22	eBioscience	46-7321
mTNF-α	APC	MP6-XT22	eBioscience	17-7321
mIFNG	PE	XMG1.2	eBioscience	12-7311
mIFNG	PE-Cy7	XMG1.2	eBioscience	25-7311
h/mCD44	FITC	IM7	eBioscience	11-0441
mNK1.1	PE	PK136	eBioscience	12-5941
mCD62L	APC	MEL-14	eBioscience	17-0621
mCD4	Per-cp-eF710	GK1.5	eBioscience	46-0041
hCD4	FITC	RPA-T4	eBioscience	11-0049
hCD3	PE-eF610	UCHT1	eBioscience	61-0038

hCD3	SB436	UCHT1	eBioscience	62-0038
hCD8a	SB436	RPA-T8	eBioscience	62-0088
hTNFA	PE-Cy7	Mab11	eBioscience	25-7349
hIFNG	APC	4S.B3	eBioscience	50-7319
hCD45RA	FITC	HI100	eBioscience	11-0458
hCD45RO	PE-Cy7	UCHL1	eBioscience	25-0457
hFOXP3	APC	PCH101	eBioscience	17-4776
h/mCD44	SB436	IM7	eBioscience	62-0441
hTNFA	PE	Mab11	eBioscience	12-7349

318

Table S3. Primers used for real-time PCR (mouse)

Genes	Forward (5'–3')	Reverse (5'–3')
Ppargc1a	GAGCTACGGGGTCGCTTC	GGGACCCCAATCTCACCT
Lonp1	TGCGGAAACGCTAC AGGAC	GGAACAGAGCCCGGTGAAGG
Clpp	AAGCCTGTAGCCCACGTCGTA	AAGGTACAACCCATCGGCTGG
Hspd1	CCTCTCTCTAATCAGCCCTCTG	GAGGACCTGGGAGTAGATGAG
Tid1	GCCCATCCTCTGTGACTCAT	AGGCCACAGGTATTTTGTCG
Chop	TCCATCCAGTTGCCTTCTTG	TTCCACGATTTCCCAGAGAAC
Atf4	TCAGCCAGATGCAGTTAACGC	TCTGGACCCATTCCTTCTTGG
Fgf21	CAAAATCTCCAACCCATGCT	CACCACCAGGGTCTTCAAGT
Tnf	ATCGCAAACAAGCTGACCTG	AGATCCAGGTTTGAGGTGGG
Rankl	CCCTTGATGAAGAGGGATCA	ACTCCACAGGTGGGAACAAG
Rorat	TCCTCCAGGGATCCAACGA	GGCAGGCGGGAGGTCTT
Rorgt	CTGGGCTACACTGAGCACC	AAGTGGTCGTTGAGGGCAATG
Il17a	GCAAGAGATCCTGGTCCTGA	AGCATCTTCTCGACCCTGAA
18s	CTGGTTGATCCTGCCAGTAG	CGACCAAAGGAACCATAACT
Oscar	TCGCTGATACTCCAGCTGTC	ATCCCAGGAGTCACAACTGC
Ctsk	GCAGGATGTGGGTGTTCAAGT	TCCAGCATTTCCTCCGGAG
Nfatc1	AATTAGGAGTGGGGGATCGT	ATCCAACCCAACTCGCCT
Acp5	CGTCTCTGCACAGATTGCAT	GAGTTGCCACACAGCATCAC
Itgb3	GGCGTTGTTGTTGGAGAGTC	CTTCAGGTTACATCGGGGTGA
Mmp9	TAGCTACCTCGAGGGCTTCC	GTGGGACACATAGTGGGAGG
Runx2	GACTGTGGTTACCGTCATGGC	ACTTGGTTTTTCATAACAGCGGA
Alpl	GGCTGGAGATGGACAAATTCC	CCGAGTGGTAGTCACAATGCC
Bmp2	TCTTCCGGGAACAGATACAGG	TGGTGTCCAATAGTCTGGTCA
Bglap	CTGACCTCACAGATCCCAAGC	TGGTCTGATAGCTCGTCACAAG
Sparc	TGGGAGAATTTGAGGACGGTG	GAGTCGAAGGTCTTGTTGTCAT

320

Table S4. Primers used for real-time PCR (human)

Genes	Forward (5'–3')	Reverse (5'–3')
CXCL12	CTGCCGCTTTGCAGGTGTA	CATTGTGGGCAAGGTGCTATT
CD44	ATTGTCCAGGCCAATACACATT	CCTCTCTACCTGCGTATCGTTTT
TNF	AAGGGGCAAAATGGTTCTTTCG	GCACCTGTATGTCCCCGAG
IL17A	TCGGTAACTGACTTGAATGTCCA	TCGCTTCCCTGTTTTAGCTGC
ACTB	CATGTACGTTGCTATCCAGGC	CTCCTTAATGTCACGCACGAT

Fig. S1

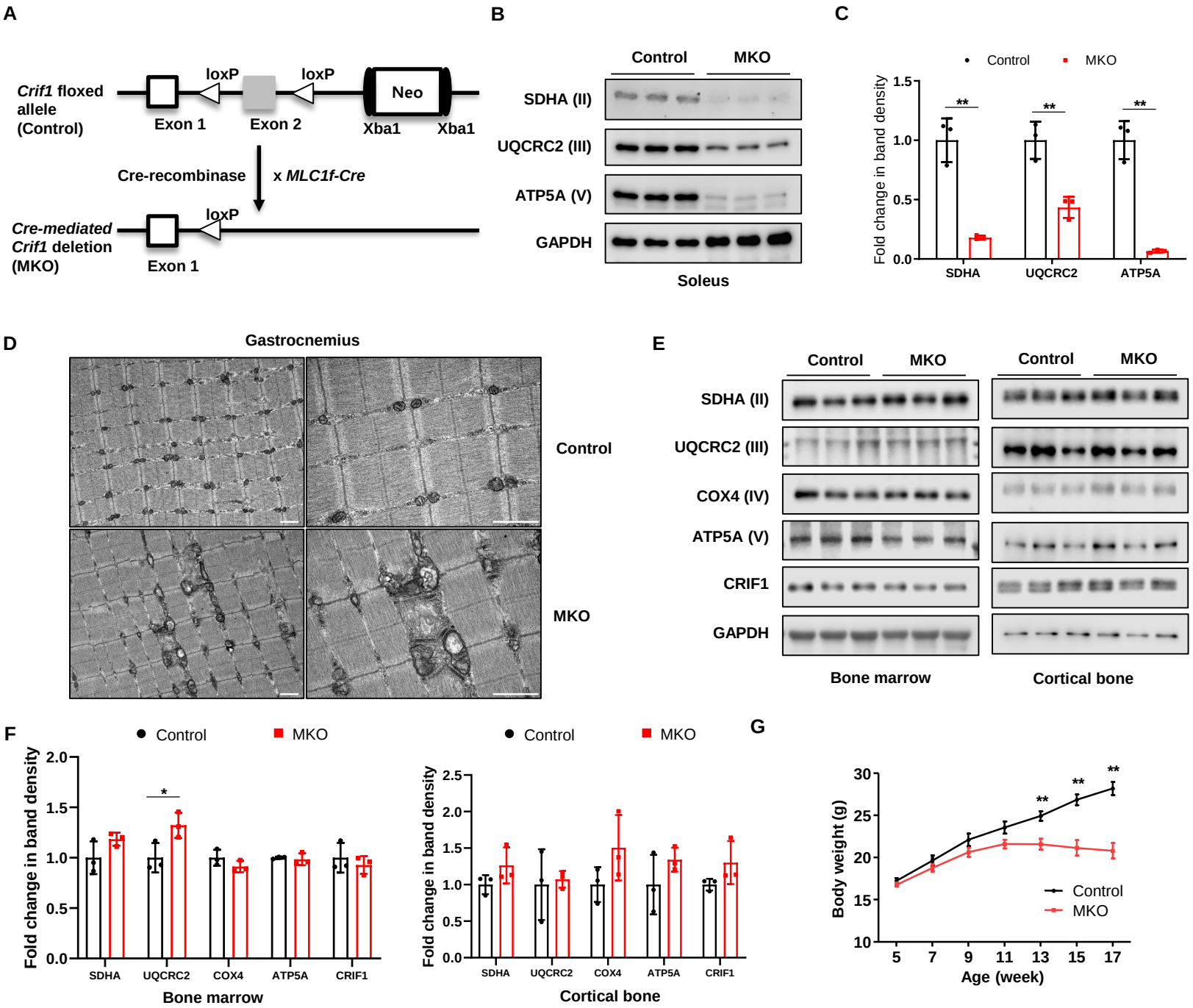
A
Crif1 floxed allele (Control)
loxP
loxP
Neo
Exon 1
Exon 2
Xba1
Xba1
Cre-recombinase
x MLC1f-Cre
Cre-mediated Crif1 deletion (MKO)
loxP
Exon 1
B
Control
MKO
SDHA (II)
UQCRC2 (III)
ATP5A (V)
GAPDH
Soleus
C
Control
MKO
Fold change in band density
1.5
1.0
0.5
0.0
**
**
**
SDHA
UQCRC2
ATP5A
D
Gastrocnemius
Control
MKO
E
Control
MKO
Control
MKO
SDHA (II)
UQCRC2 (III)
COX4 (IV)
ATP5A (V)
CRIF1
GAPDH
Bone marrow
Cortical bone
F
Control
MKO
Fold change in band density
2.0
1.5
1.0
0.5
0.0
*
SDHA
UQCRC2
COX4
ATP5A
CRIF1
Bone marrow
Control
MKO
Fold change in band density
2.5
2.0
1.5
1.0
0.5
0.0
SDHA
UQCRC2
COX4
ATP5A
CRIF1
Cortical bone
G
Body weight (g)
30
25
20
15
10
**
**
**
Control
MKO
5
7
9
11
13
15
17
Age (week)

Fig. S2

A

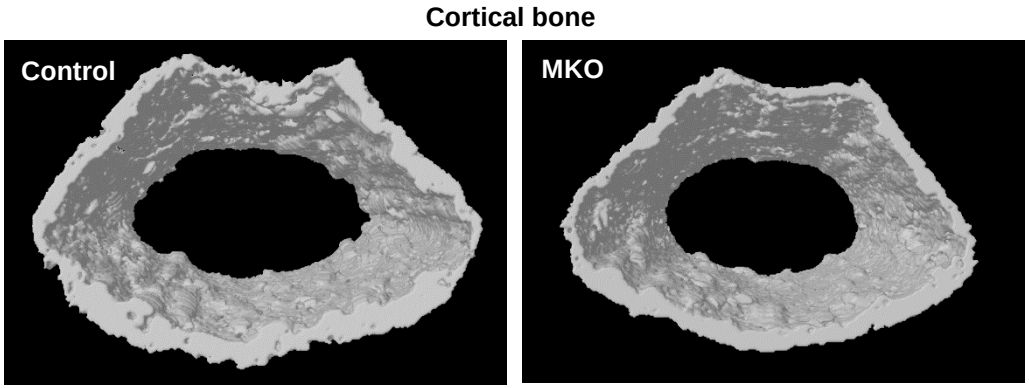

B

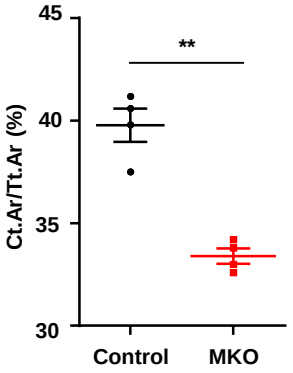

C

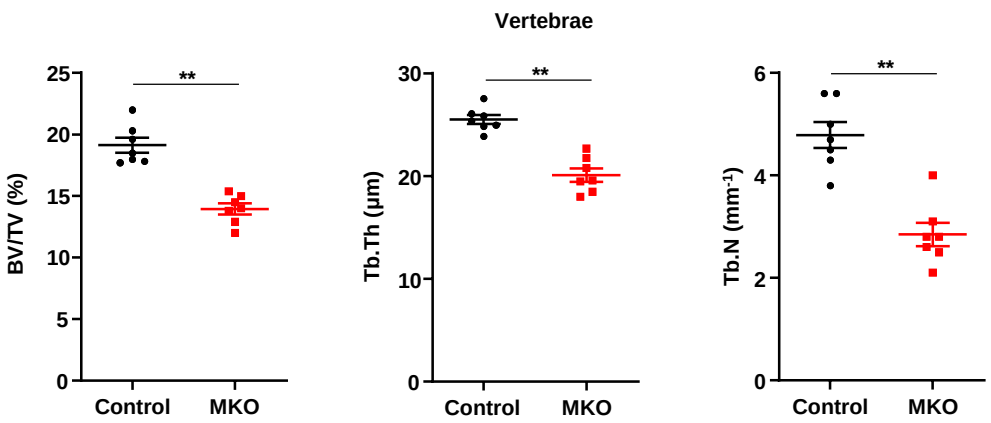

E

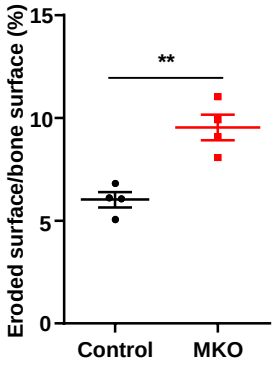

D

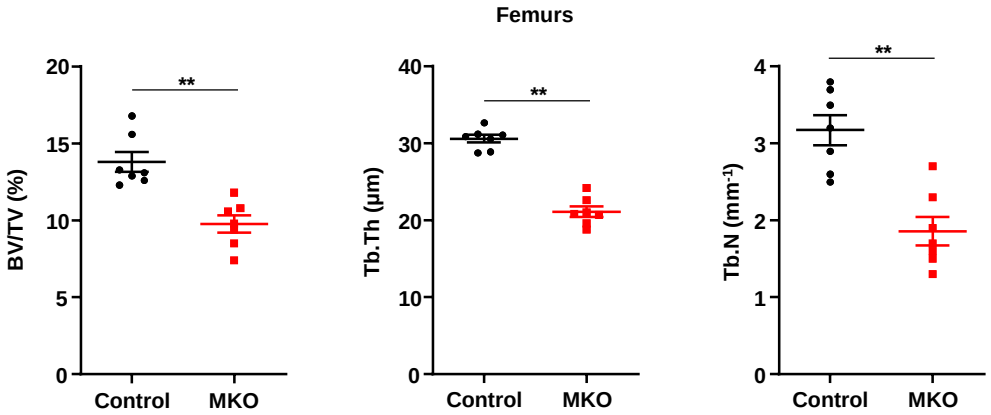

F

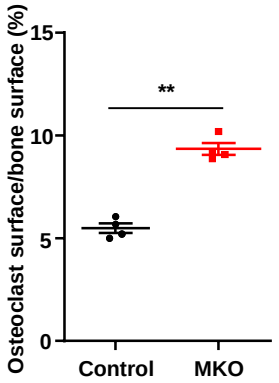

Fig. S3

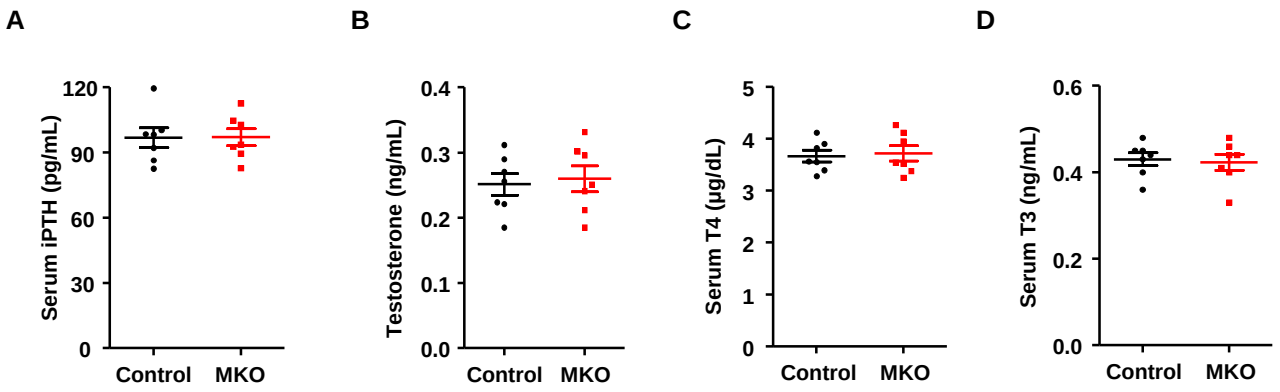
A
Serum iPTH (pg/mL)
120
90
60
30
0
Control
MKO
B
Testosterone (ng/mL)
0.4
0.3
0.2
0.1
0.0
Control
MKO
C
Serum T4 (μg/dL)
5
4
3
2
1
0
Control
MKO
D
Serum T3 (ng/mL)
0.6
0.4
0.2
0.0
Control
MKO

Fig. S4

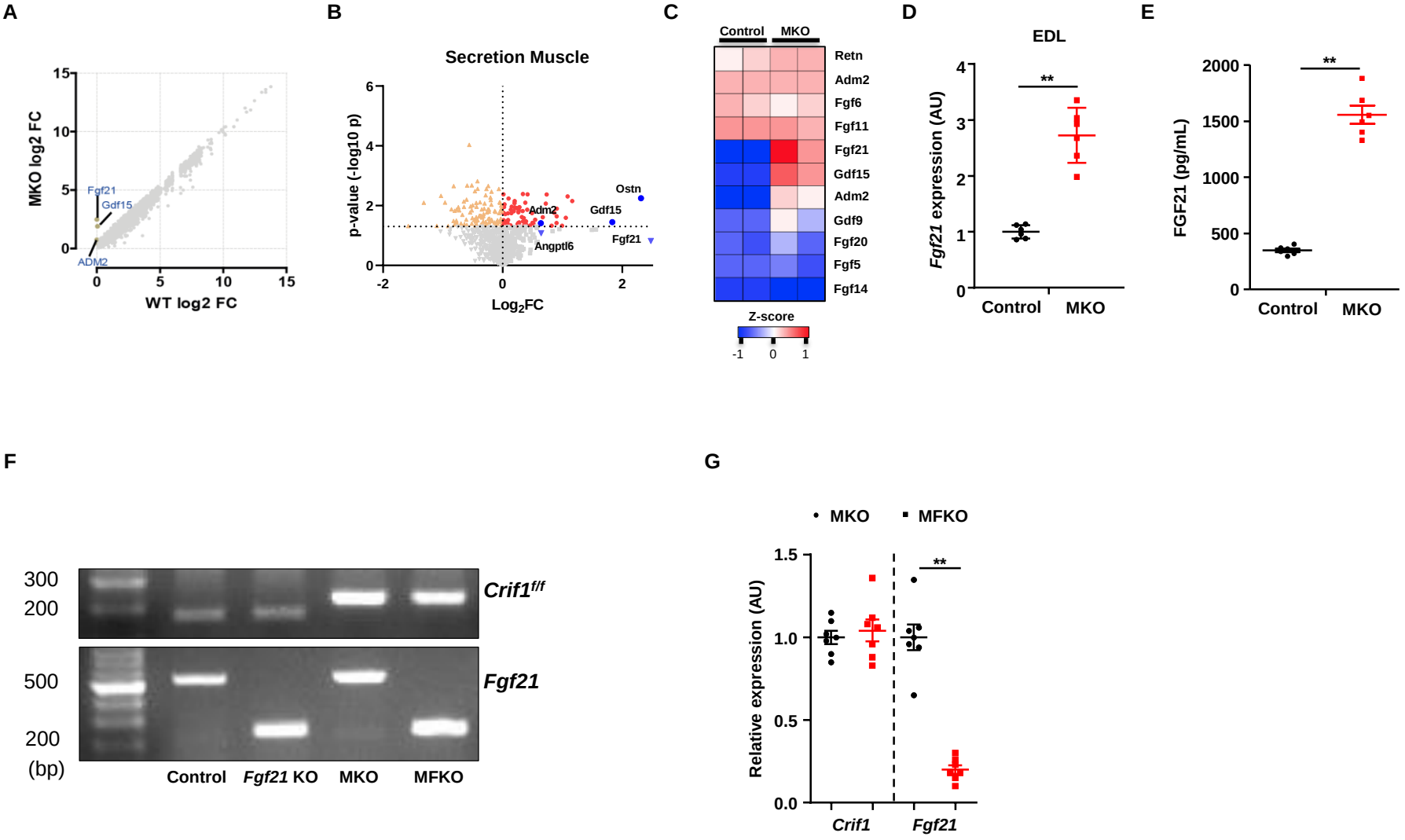
A
MKO log2 FC
WT log2 FC
Fgf21
Gdf15
ADM2
B
Secretion Muscle
p-value (-log10 p)
Log2FC
Ostn
Adm2
Gdf15
Fgf21
Angptl6
C
Control
MKO
Retn
Adm2
Fgf6
Fgf11
Fgf21
Gdf15
Adm2
Gdf9
Fgf20
Fgf5
Fgf14
Z-score
D
EDL
Fgf21 expression (AU)
Control
MKO
E
FGF21 (pg/mL)
Control
MKO
F
Crif1f/f
Fgf21
(bp)
Control
Fgf21 KO
MKO
MFKO
G
MKO
MFKO
Relative expression (AU)
Crif1
Fgf21

Fig. S5

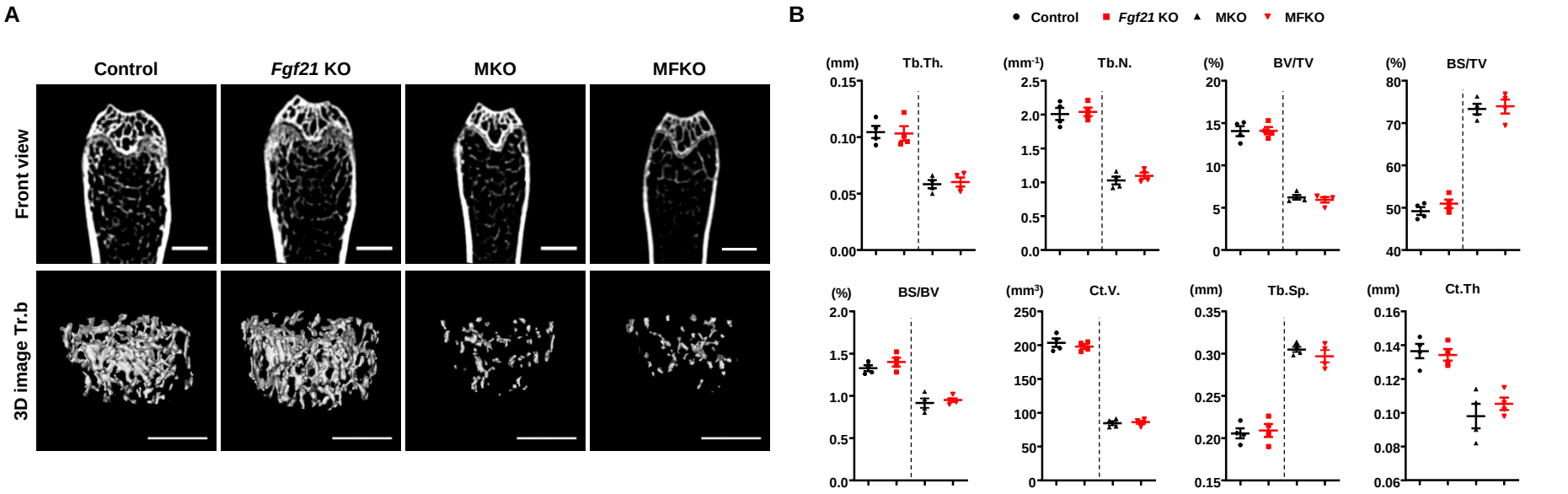
A
Control
Fgf21 KO
MKO
MFKO
Front view
3D image Tr.b
B
Control
Fgf21 KO
MKO
MFKO
(mm) Tb.Th.
(mm-1) Tb.N.
(%) BV/TV
(%) BS/TV
(%) BS/BV
(mm3) Ct.V.
(mm) Tb.Sp.
(mm) Ct.Th

A

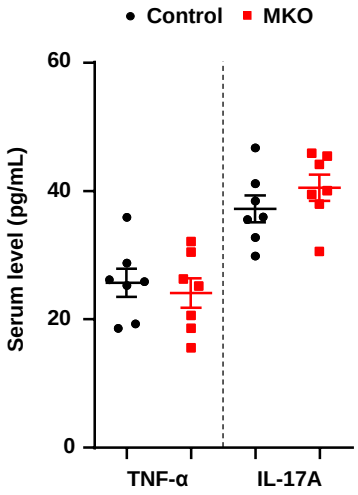
Control
MKO
Serum level (pg/mL)
60
40
20
0
TNF-α
IL-17A

B

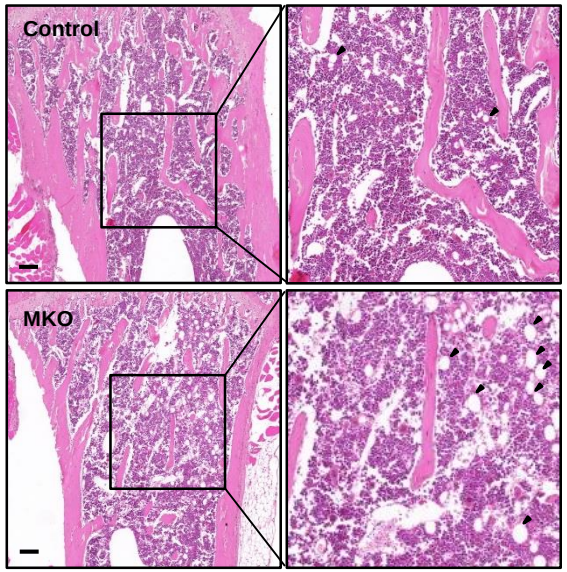
Control
MKO

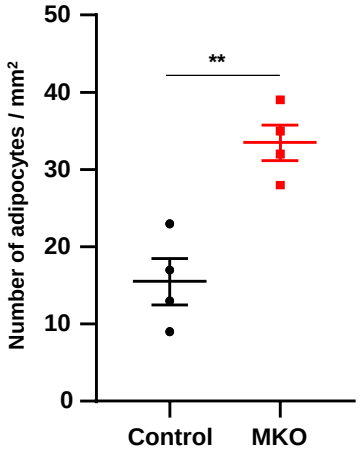
Number of adipocytes / mm²
50
40
30
20
10
0
**
Control
MKO

A

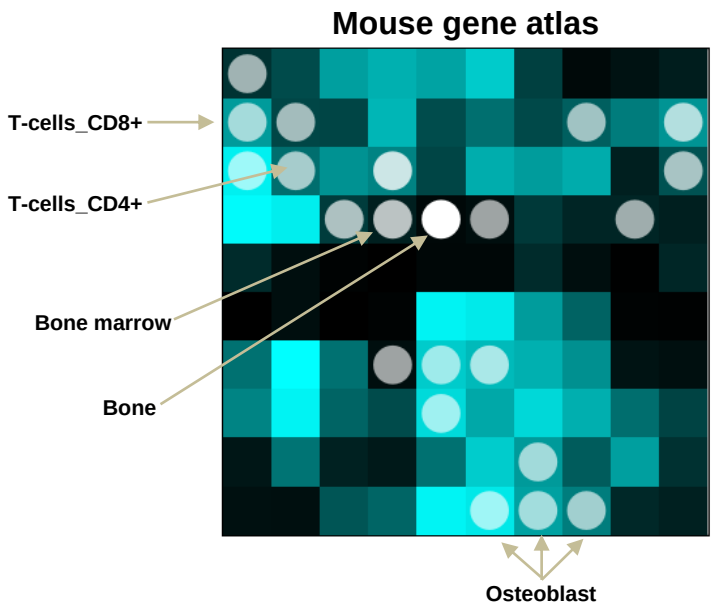
Mouse gene atlas
T-cells_CD8+
T-cells_CD4+
Bone marrow
Bone
Osteoblast

B

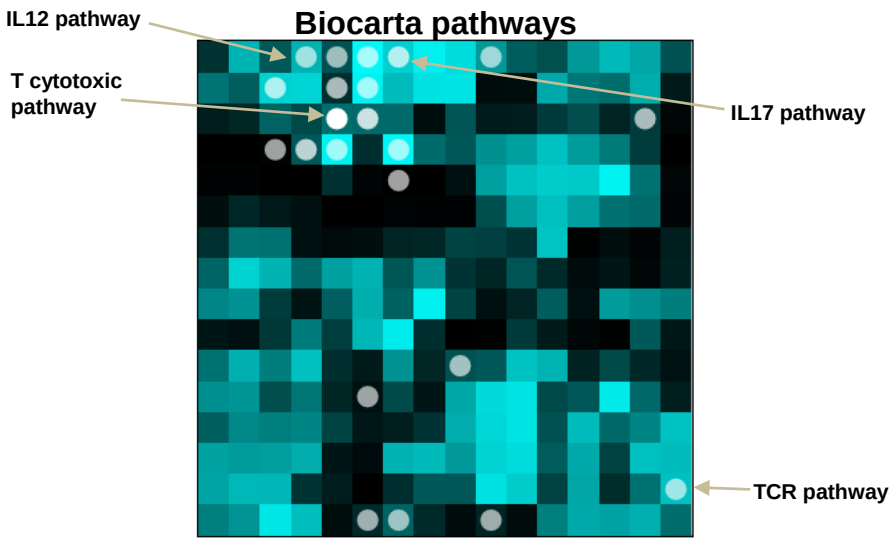
Biocarta pathways
IL12 pathway
T cytotoxic pathway
IL17 pathway
TCR pathway

C

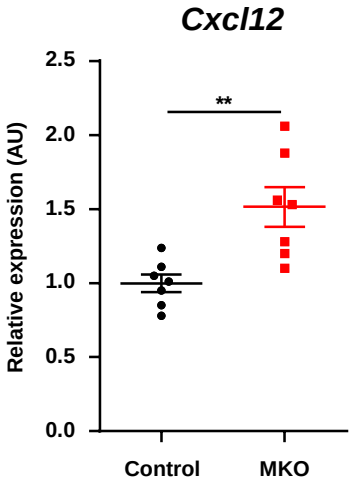
Cxcl12
Relative expression (AU)
2.5
2.0
1.5
1.0
0.5
0.0
**
Control
MKO

D

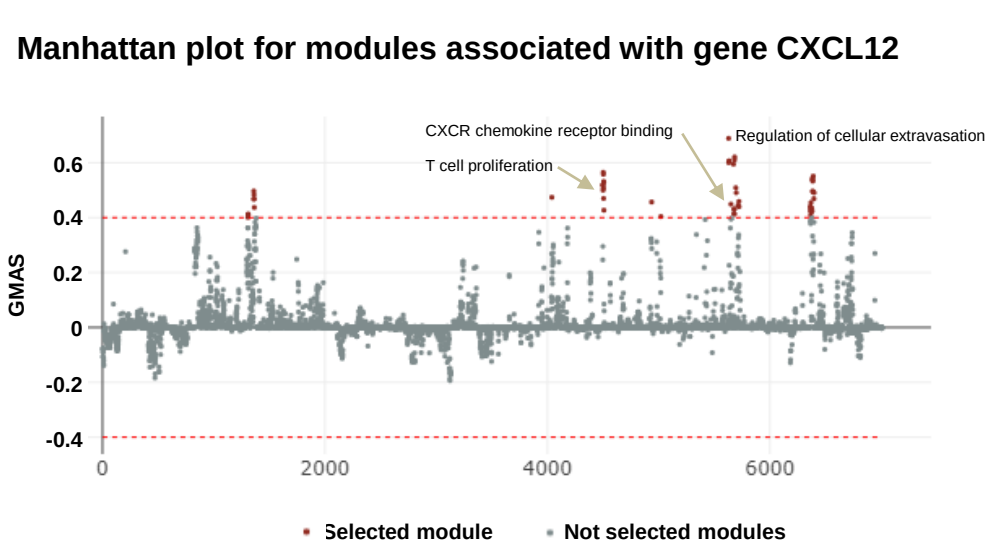
Manhattan plot for modules associated with gene CXCL12
CXCR chemokine receptor binding
Regulation of cellular extravasation
T cell proliferation
GMAS
0.6
0.4
0.2
0
-0.2
-0.4
0
2000
4000
6000
Selected module
Not selected modules

Fig. S8

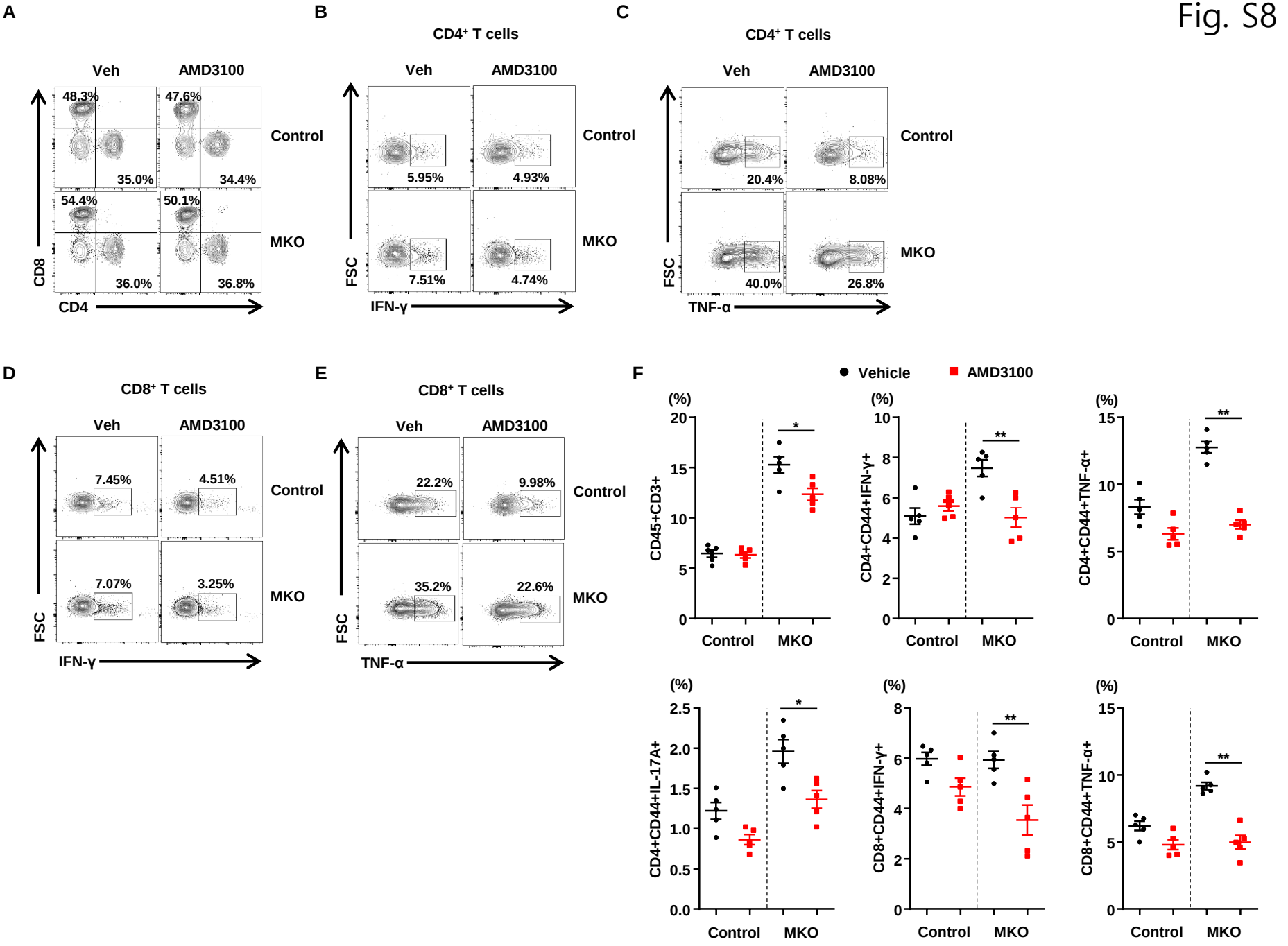
A
Veh
AMD3100
48.3%
47.6%
35.0%
34.4%
54.4%
50.1%
36.0%
36.8%
Control
MKO
CD8
CD4
B
CD4+ T cells
Veh
AMD3100
5.95%
4.93%
7.51%
4.74%
Control
MKO
FSC
IFN-γ
C
CD4+ T cells
Veh
AMD3100
20.4%
8.08%
40.0%
26.8%
Control
MKO
FSC
TNF-α
D
CD8+ T cells
Veh
AMD3100
7.45%
4.51%
7.07%
3.25%
Control
MKO
FSC
IFN-γ
E
CD8+ T cells
Veh
AMD3100
22.2%
9.98%
35.2%
22.6%
Control
MKO
FSC
TNF-α
F
Vehicle
AMD3100
(%)
CD45+CD3+
CD4+CD44+IFN-γ+
CD4+CD44+TNF-α+
CD4+CD44+IL-17A+
CD8+CD44+IFN-γ+
CD8+CD44+TNF-α+
Control
MKO
*
**

Fig. S9

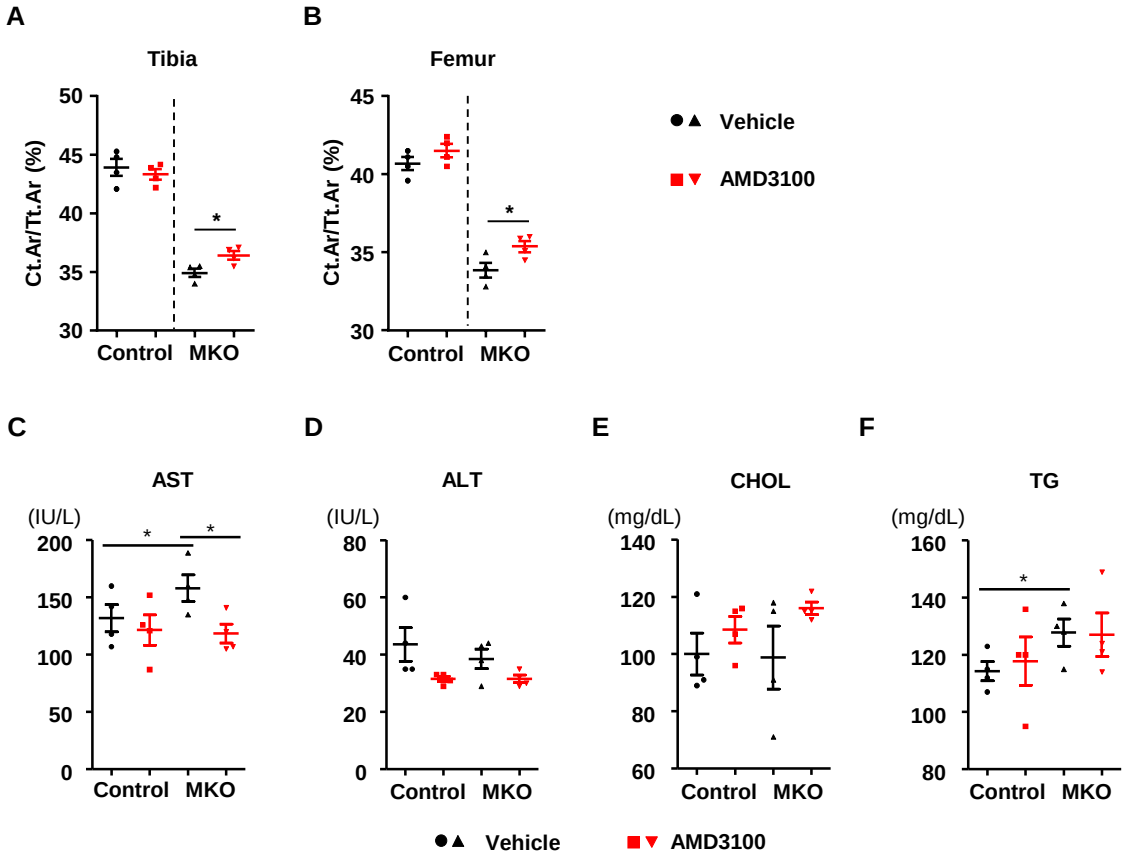
A
Tibia
Ct.Ar/Tt.Ar (%)
50
45
40
35
30
Control
MKO
*
B
Femur
Ct.Ar/Tt.Ar (%)
45
40
35
30
Control
MKO
*
Vehicle
AMD3100
C
AST
(IU/L)
200
150
100
50
0
Control
MKO
*
*
D
ALT
(IU/L)
80
60
40
20
0
Control
MKO
E
CHOL
(mg/dL)
140
120
100
80
60
Control
MKO
F
TG
(mg/dL)
160
140
120
100
80
Control
MKO
*
Vehicle
AMD3100

Fig. S10

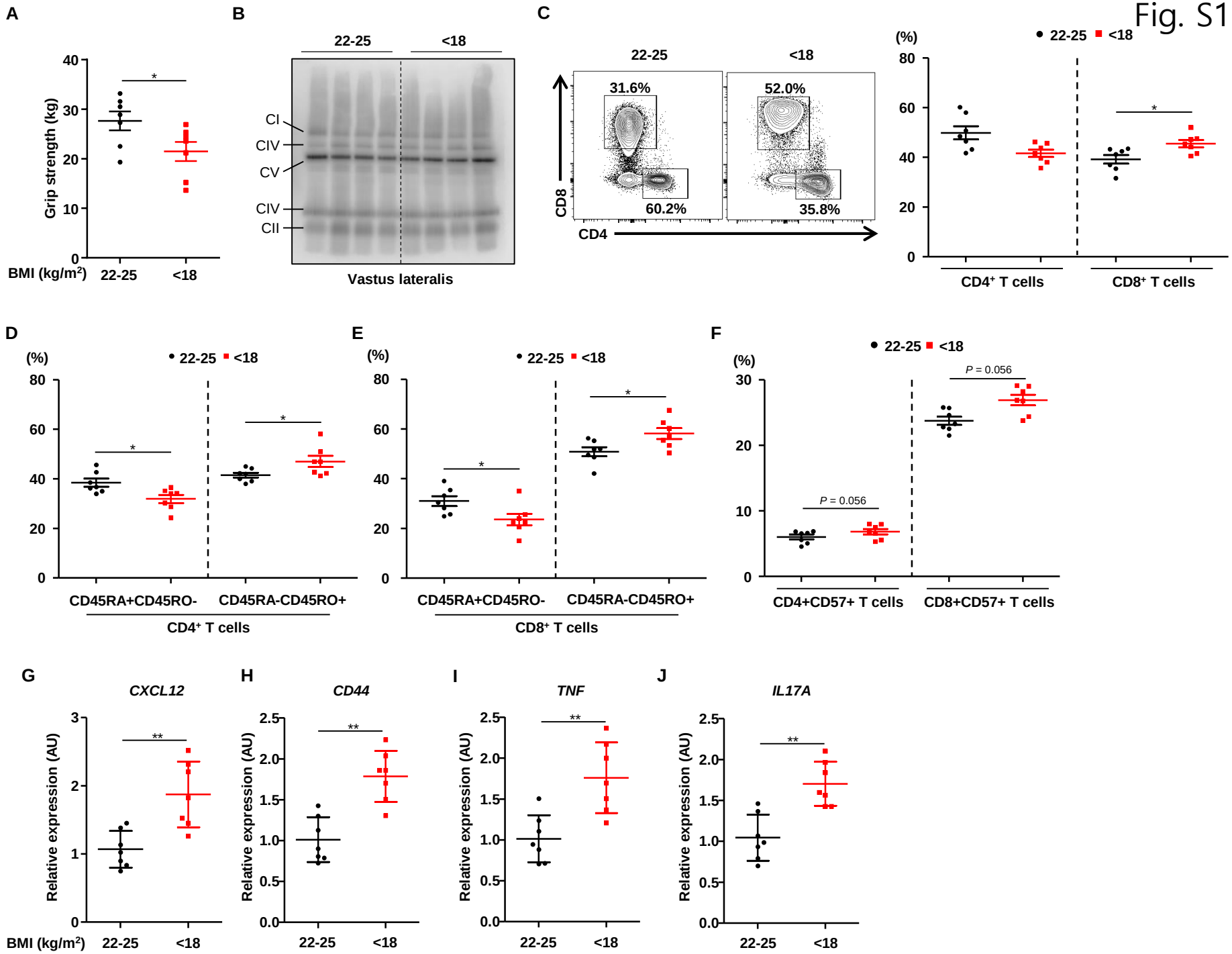
A
Grip strength (kg)
BMI (kg/m²)
22-25
<18
B
22-25
<18
CI
CIV
CV
CIV
CII
Vastus lateralis
C
22-25
<18
31.6%
52.0%
60.2%
35.8%
CD8
CD4
(%)
22-25
<18
CD4⁺ T cells
CD8⁺ T cells
D
(%)
22-25
<18
CD45RA+CD45RO-
CD45RA-CD45RO+
CD4⁺ T cells
E
(%)
22-25
<18
CD45RA+CD45RO-
CD45RA-CD45RO+
CD8⁺ T cells
F
(%)
22-25
<18
P = 0.056
P = 0.056
CD4+CD57+ T cells
CD8+CD57+ T cells
G
CXCL12
Relative expression (AU)
BMI (kg/m²)
22-25
<18
H
CD44
Relative expression (AU)
22-25
<18
I
TNF
Relative expression (AU)
22-25
<18
J
IL17A
Relative expression (AU)
22-25
<18

Fig. S11

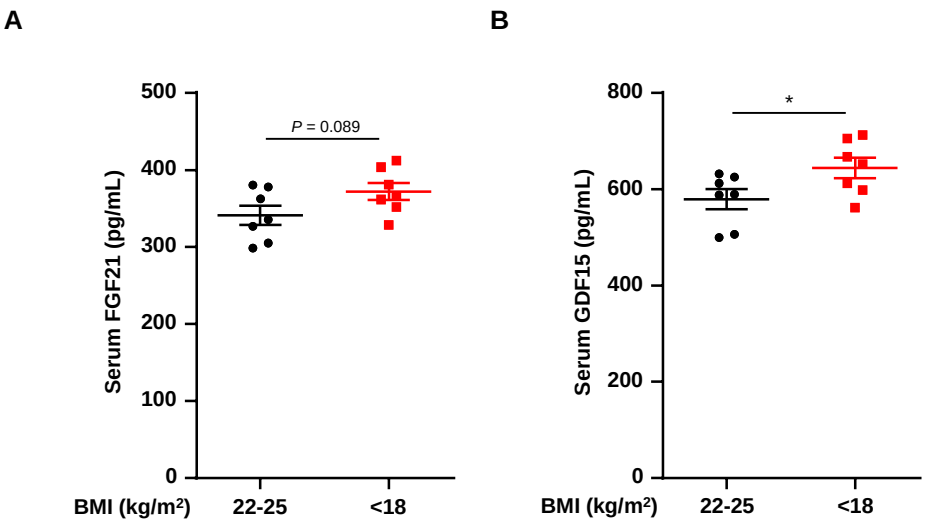
A
B
500
400
300
200
100
0
Serum FGF21 (pg/mL)
P = 0.089
BMI (kg/m²)
22-25
<18
800
600
400
200
0
Serum GDF15 (pg/mL)
*
BMI (kg/m²)
22-25
<18